Electrodeposition and Behavior of Single Metal Nanowire Probes

Munekazu Motoyama[†,§,*] and Friedrich B. Prinz[†,‡]

[†]Department of Mechanical Engineering, Stanford University, Stanford, California 94305, United States and [‡]Department of Materials Science & Engineering, Stanford University, Stanford, California 94305, United States. [§]Present address: Department of Materials, Physics and Energy, Nagoya University, Furo-cho, Chikusa-ku, Nagoya, 464-8603 Japan.

ABSTRACT This paper describes the fabrication of scanning probes with single metal nanowires (NWs) at the probe tip. The porous-template technique can produce NWs of various kinds of metals, with diameters down to 10−20 nm, which compete with multiwall carbon nanotube diameters. Metal NWs are grown by electrodeposition on the scanning probe tip. One NW can be selected to remain by focused ion beam technique. A variety of metals can be chosen as the tip material. Electric potentials of NWs at the probe tip can be measured. Single NW probes can measure surface topographies, electrode potentials, and their mechanical bending properties.

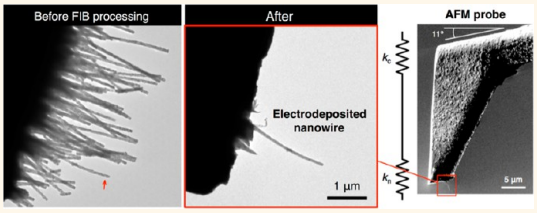

KEYWORDS: electrodeposition · porous template · single metal nanowire · atomic force microscopy · focused ion beam

Nanoporous-template films can be used for electrodeposition of various one-dimensional (1-D) nanostructures.[1−4] Many authors have exploited the porous-template method using porous anodic alumina or polycarbonate-track-etched membranes. Many interesting applications have been proposed.[5−7] To produce arrays of 1-D nanostructures, the porous-template method is a powerful technique. However, significant challenges remain in creating single nanowire (NW) tools from porous templates.[7,8]

This study aims to apply electrodeposited single metal NWs to scanning probe technology. The porous-template method can produce NWs with diameters down to 10−20 nm.[9] These diameter values are comparable to those of multiwall carbon nanotubes (MWCNTs). CNT atomic force microscope (AFM) probes have already been commercialized with MWCNTs. However, CNT tips must be subsequently coated with a metal layer for conductive probe applications. Moreover, there is the risk of wearing off the metal coating due to limited interfacial strength between the CNT and metal layer. Using an all-metal NW for a scanning probe tip is thought to address these issues, *i.e.*, retaining a sufficiently small tip radius without the risk of demetalizing the tip.

There are only a few techniques for growing a single metal NW at a desired position. Ion-beam-induced deposition allows for vertical growth of single NWs at desired positions. Alternatively, pulling out a Ag_2Ga alloy NW from Ga liquid with a Ag-coated AFM probe is a possible technique for producing single-NW probes.[10] However, the presence of Ga typically contained in a significant fraction of the metal NWs narrows the possible range of applications. Furthermore, material choices are very limited. Electrodeposition can be applied to many kinds of metals.[11]

The mechanical properties of NWs have also attracted significant interest.[12−14] With a single metal NW vertically attached to the tip of an AFM probe, several kinds of mechanical tests with forces on the order of pico- to nanonewton can be consistently conducted for the same NW until it breaks. Therefore, NW probes can be versatile tools.

Previous work demonstrated electrodepositon of metal NWs on the tip of AFM probes.[15] However, the probe structure was not a single-NW probe. Moreover, the wire diameters were not yet of sufficiently small values. Here, we report on the novel fabrication method of a single-metal-NW scanning probe and demonstrate several probe functions.

* Address correspondence to munekazu@numse.nagoya-u.ac.jp.

Received for review December 30, 2013 and accepted March 4, 2014.

Published online March 04, 2014
10.1021/nn4066582

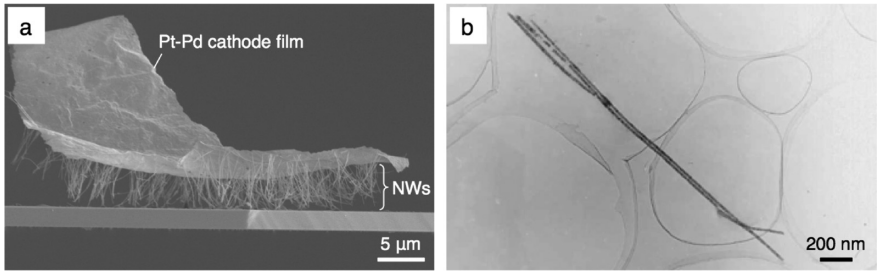

Figure 1. (a) SEM and (b) transmission electron microscope (TEM) images of NWs produced by electrodeposition using polycarbonate membranes with 15-nm-diameter pores. The Pt–Pd film in (a) was the cathode for growing NWs.

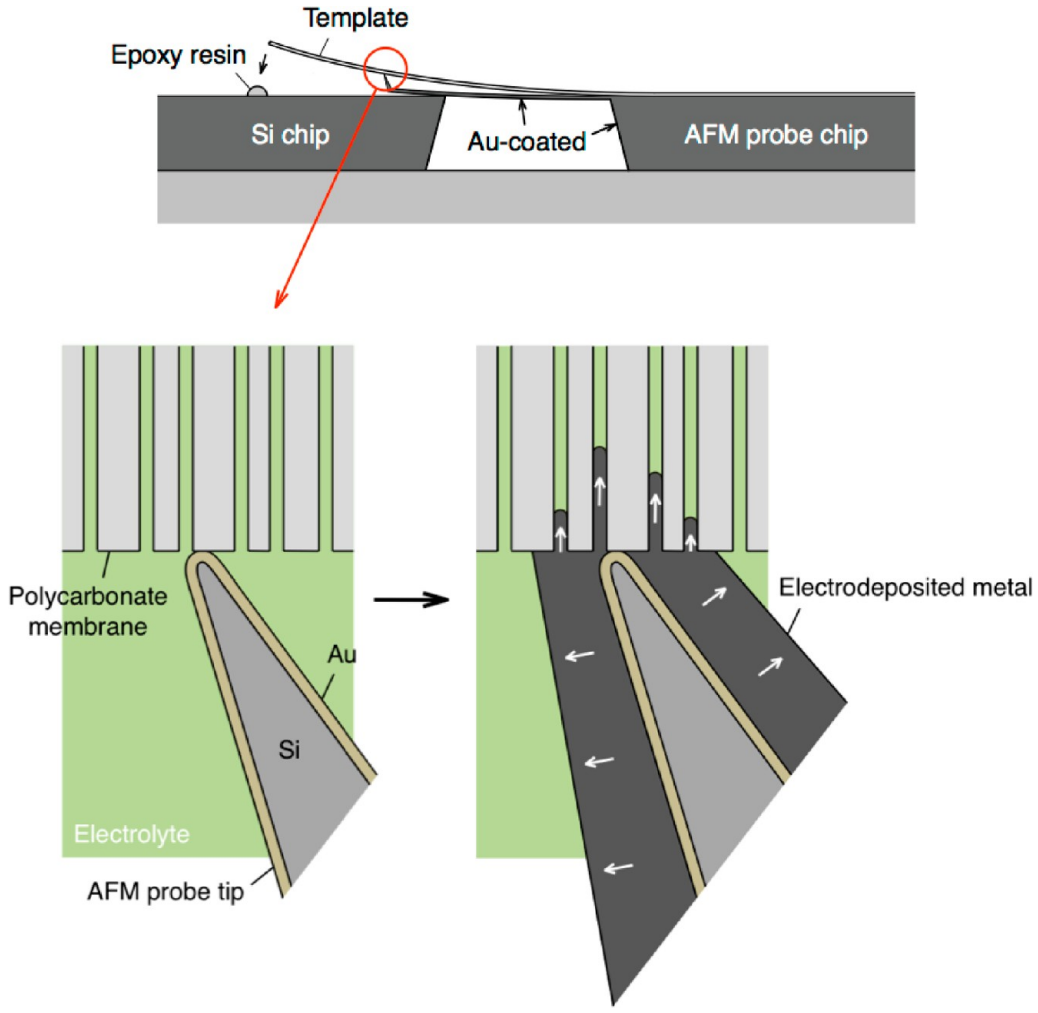

Figure 2. Schematic illustrations of the Au-coated tip of an AFM probe contacting a porous polycarbonate membrane. An AFM probe with a tip facing up is attached to a Cu plate. A Si chip is also fixed to support a cantilever beam from below. An edge of a membrane is immobilized on a Si chip with epoxy resin. These AFM probe and Si chip attached to a Cu plate are immersed in an electrolyte and grow NWs into pores from the probe tip by electrodeposition.

RESULTS AND DISCUSSION

Single-Metal-NW Probes. Figure 1a shows a scanning electron microscope (SEM) image of Ni NWs produced by electrodeposition into a polycarbonate membrane with 15-nm-diameter pores. The template membrane for the NWs in Figure 1a was completely removed by air-plasma etching. Electrodeposited NWs had the same diameter as the membrane pores with diameters of 15 nm, as confirmed in previous work (Figure 1b).[9]

Figure 2 illustrates how NWs were electrodeposited on the AFM probe tip. A template membrane and a probe were coupled with epoxy resin. A same-height Si chip was placed underneath a cantilever beam. An edge of a membrane covering a probe tip was also fixed at a Si chip with epoxy resin. The Au-coated-probe tip supported the underside of a membrane. Electrodeposition started on the entire surface of the Au cathode. Metal NWs grew into pores toward the other

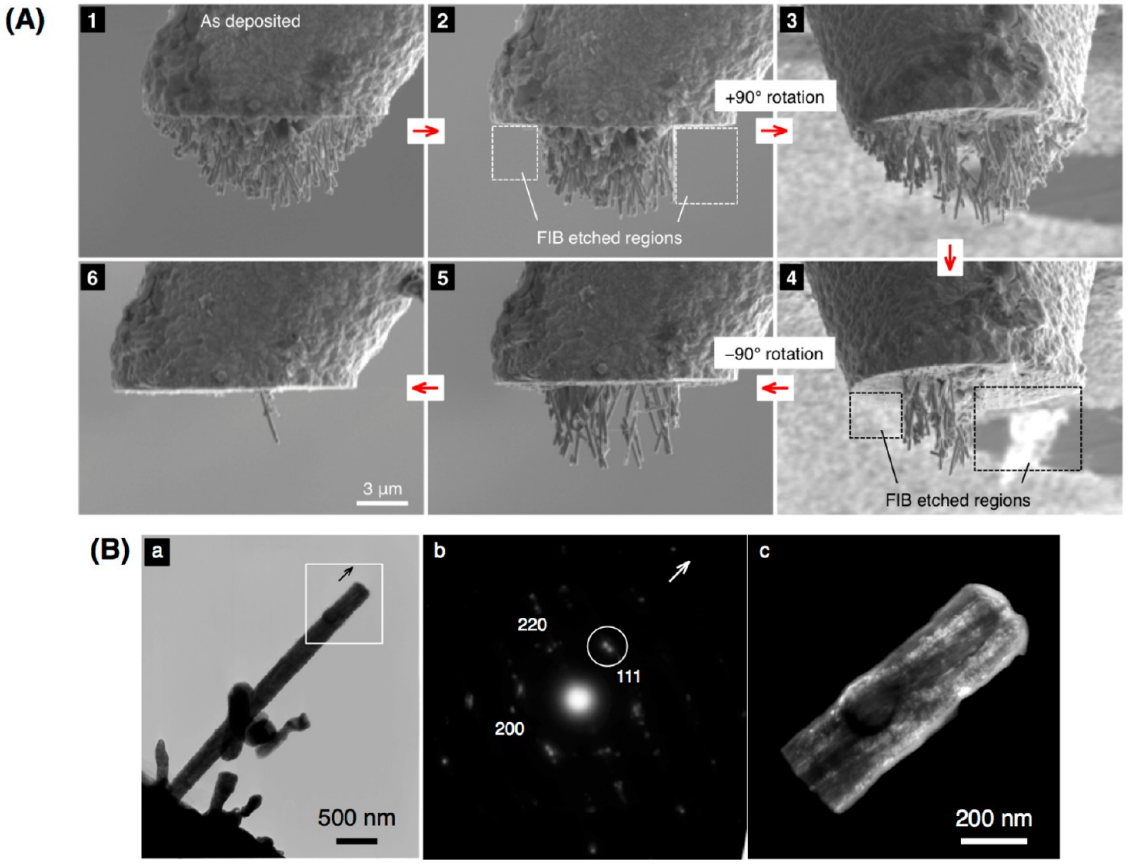

Figure 3. (A) Sequential SEM images of FIB processing to remove Ni NWs from the probe tip except one in the center. (1) Deposited NWs after dissolving a template membrane. (2, 4) After ion-beam etching in dotted-line-square regions. (3) +90-degree-rotated specimen. (5) Specimen in the original configuration. (6) A single NW left on the tip. (B) TEM image of the Ni NW in (A-6). (a) Bright-field image. (b) Electron diffraction pattern from the square at the tip in (a). An arrow indicates the NW longitudinal direction. (c) Dark-field image using the 111 diffraction spot in the circle in (b).

end of the membrane, and a metal film also grew on a probe.

For scanning probe microscope applications, only one vertical wire was needed at the tip. This study applied the focused ion beam (FIB) technique to leave one wire by removing the other deposited wires. Accelerated ion beam particles etched the sample surface and, in response, surface atoms gained sufficiently high kinetic energy to be removed from the surface.[16] If we attempted to remove NWs by vertical ion beams, sputtered particles were redeposited on the surfaces of the remaining NWs.[17] The diameter of remaining wires became larger during etching. To minimize such redeposition, ion beams were always pointed from a direction perpendicular to the wires.

An SEM image in Figure 3A-1 shows a side view of Ni NWs deposited on the probe tip after a membrane was removed. The nominal diameter of membrane pores was 100 nm. The wires deposited nearer to the edges were shorter because the wires nearer to the edges started to grow later than ones nearer to the center (see Figure 2).[15] The growth rate estimated from the wire in the center at the tip (5.4 μm in length) was 36 nm s^{-1}.

Figure 3A-2 to 6 shows SEM images of each sequential etching step of leaving one wire on the probe tip. The first step was to irradiate ion beams with a small current to eliminate wires only in the outermost regions on the base (Figure 3A-2). After the ion beams completely etched the wires, the beams did not hit anything behind the wires, in contrast to the case where beams were directed from the top. Next, the specimen was rotated by 90° (Figure 3A-3). Likewise, wires on the sides were etched (Figure 3A-4). The specimen was returned to the original configuration (Figure 3A-5). By repeating these steps, the number of wires on the tip can be reduced eventually down to one. Figure 3A-6 shows an SEM image of the probe tip with a single NW.

Figure 3B-a shows a TEM image of the single NW at the tip. A small piece of another wire was attached to the middle of the single wire. This was because the paths of cylindrical pores diagonally penetrate a template membrane, whereby some pores partially collide with others to merge into complex profiles. This problem can be minimized by selecting the best single wire at the tip in the etching step.

An electron diffraction pattern from the NW tip (Figure 3B-a, b) using a TEM shows significant diffuse

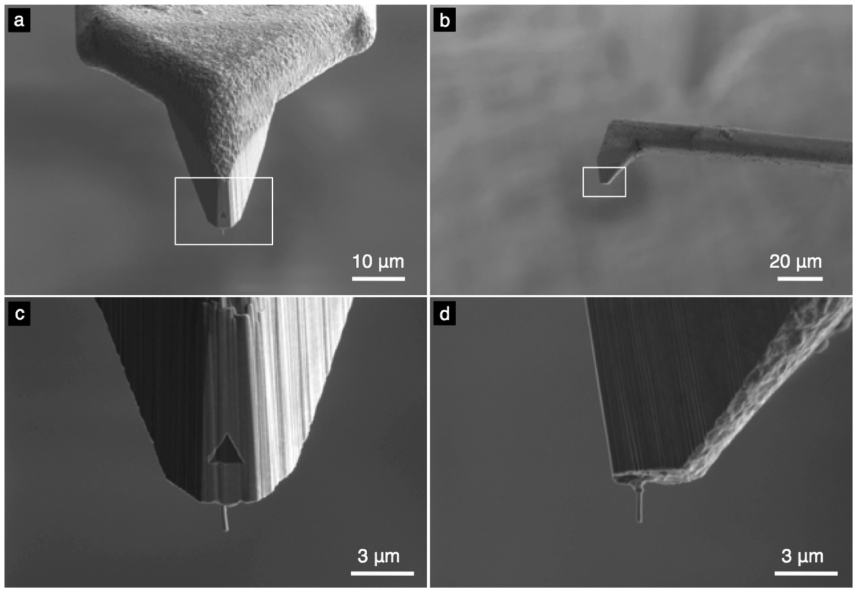

Figure 4. SEM images of a single-NW probe with the front part trimmed by FIB. The dark triangle in the front views in (a) and (c) is exposed Si surface. (b, d) Side views.

scattering perpendicular to the arrow, indicating the presence of many microtwins or stacking faults along the NW length. A dark-field image taken from the 111 diffraction spots encircled in Figure 3B-b is shown in Figure 3B-c. Grains with the same orientation tend to be parallel to the NW longitudinal direction. Energy dispersive X-ray spectroscopy (EDS) analysis indicated that Ga contaminants on surfaces were suppressed to be only 2 at. %. The wire tip diameter is, in fact, 250 nm, which is greater than the nominal diameter of 100 nm. It is known that pores of commercial-polycarbonate-track-etched membranes have larger diameters inside membranes.[9,18,19] Hence, diameters in the middle of pores are larger than at the ends, where nominal values are observed.

As described above, electrodeposition also occurs outside a membrane, resulting in a widening of a probe. The front of a probe was ion-beam-etched in Figure 4. Figure 4a, c shows the front view. Figure 4b, d shows side views.

Figure 5 shows a potential transient when the tip of a single-NW probe is in contact with a 0.1 M KCl electrolyte (conductivity: 1.3×10^{-2} S cm^{-1}) on a flat Ni sheet. The *in situ* optical microscope pictures are also presented. Initially, the tip entirely contacts the electrolyte. The potential difference between a Ni sheet and a NW probe is measured. Subsequently, the electrolyte evaporates and detaches off from the tip in the optical microscope view. However, the electrode potential is still measurable. This observation indicates that only the NW tip is wet by the electrolyte (the inset illustration). The potential value gradually increases because the electrical resistance of the electrolyte bridge increases. Eventually, the potential is out of the measurable range as indicated by the red arrow in Figure 5. This measurement demonstrates that the NW at the tip is not electrically isolated. Since there was no significant difference in the growth rate of NWs on the AFM tip and into large-area membranes at the same potential in previous work,[15] the electrical resistance through a metal layer on a 450-μm-long cantilever was negligible. The electrical resistance of the single NW at the tip in this measurement was less than 10 Ω based on the bulk Ni electrical conductivity (*i.e.*, 1.4×10^5 S cm^{-1}).

Metal NW Probes with Diameters Smaller than 50 nm. We subsequently fabricated NW probes using template membranes with pores of 15 nm in diameter. Figure 6A shows SEM images of polycarbonate-track-etched membranes with 15-nm-diameter pores etched by air plasma for 0 to 45 s at a constant radiofrequency (RF) power. The profiles of openings become more conical with etching duration.[20] Figure 6B shows mouth diameters increase with etching duration. NWs with base diameters of 15 nm cannot stand free from a membrane support due to mechanical weakness. Using a membrane with conically shaped pores can grow NWs with larger base diameters while retaining sharp tip diameters.

Figure 7A shows SEM images of a NW probe produced from a plasma-etched membrane. The original pore diameters were 15 nm, before plasma treatment. No wires remained to stand on a substrate after stripping a membrane if plasma treatment was not conducted for this pore size of membranes. It was observed that the base diameters of wires were larger than the tip diameters. The length of the longest NW in the center was 5.7 μm. This was close to the length of the longest NW in Figure 3A. Hence, the length of NWs is reproducible and can be well controlled by the potential regardless of wire diameter. TEM images of a

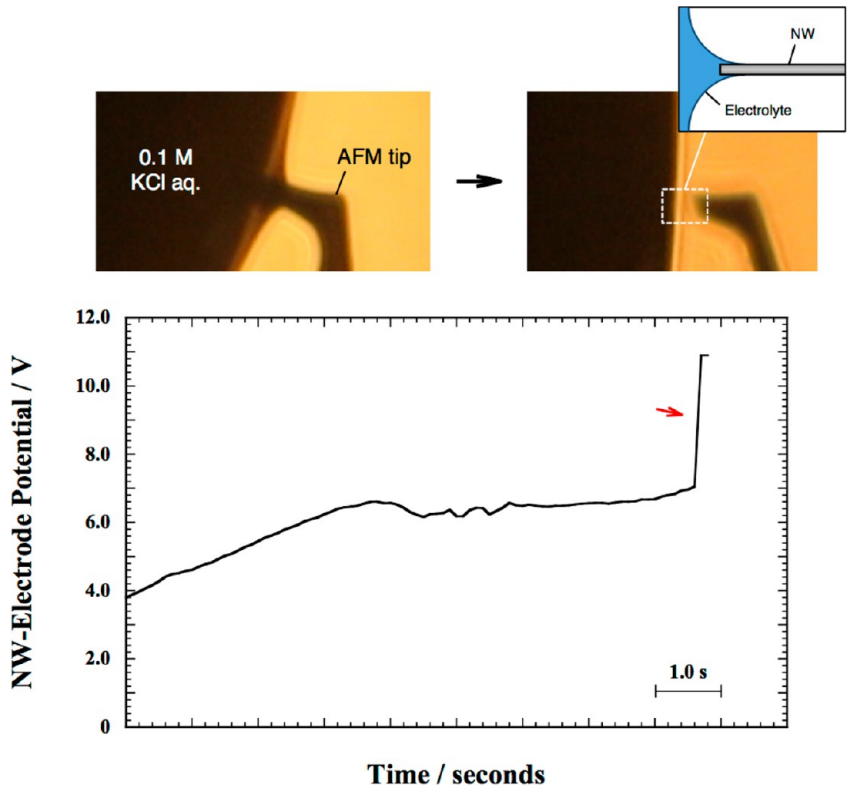

Figure 5. Potential transient measured by the tip of a NW wet by 0.1 M KCl aqueous electrolyte. The arrow indicates the moment that the electrolyte surface detached from the NW tip.

specimen before FIB etching are shown in Figure 7B-a, b. Figure 7B-b shows the tip of the wire indicated by the arrow in Figure 7B-a. The tip radius is 10−30 nm. Only a few Ni crystallites were observed at any cross section of the wire. Figure 7B-c shows the selected NW after the FIB etching. The wire kept the same diameter as before FIB etching (c and d). Previous work reported metal wires with 15-nm diameter, electrodeposited *via* porous templates as used in Figure 6.[9] Membrane templates are as thick as 6 μm. Accordingly, we can build metal NWs with aspect ratios as high as 10^2.

Normal stress at any cross section of a single wire with a point load at the free end is given by the following equation.[21]

$$\sigma_x = \frac{32Fx}{\pi\left[d_A + (d_B - d_A)\left(\frac{x}{L}\right)^n\right]^3} \quad (1)$$

where F is a point load at the free end, x is a distance in the axial direction from the free end, d_A is the free-end diameter, d_B is the base diameter, and L is the length of a wire. n is a parameter determining the shape profile of a wire. The NW in the TEM picture in Figure 7B-d has d_A = 70 nm, d_B = 230 nm, L = 2.2 μm, n = 9. All these parameters are determined from SEM and TEM observations. The reason that d_A is larger than 15 nm is the pore diameter extension inside a membrane, as mentioned above.

The range of the first-harmonic resonance frequencies of original probes was 7−25 kHz according to the manufacturer. Even after NWs were electrodeposited, the resonance frequency appeared. The first-harmonic resonance frequency of a produced NW probe was 48.2 kHz in dried air at room temperature. The quality factor was 83. Thus, the resonance frequency was slightly shifted with electrodeposition, probably because the mass of a probe was increased by deposited Ni. A spring constant of 1.7 N m^{-1} is estimated by Sader's method.[22]

Figure 8 shows contact-mode AFM images of a sample with square holes with pitches of 10 μm and depths of 200 nm. A commercial Si probe and a NW probe were used for Figure 8a and b, respectively. Scan rates were 0.5 Hz per line. Height profiles near step edges are shown in the bottom figure. A step edge appeared significantly more sharply with a NW probe than with a Si probe. The width of the step edge did not vary depending on scan direction (left-to-right or right-to-left) and the side of a hole (right or left) when the same probe was used. The aspect ratio of a NW used for this imaging was approximately 30 (see Figure 7B-d). The tip radius of a brand new Si probe (<5 nm) was smaller than the tip radius of a NW. However, the apex angles of Si probes were mostly greater than 30 degrees, whereby a high-aspect-ratio NW probe surpassed a Si probe in reaching the bottom of vertical walls.

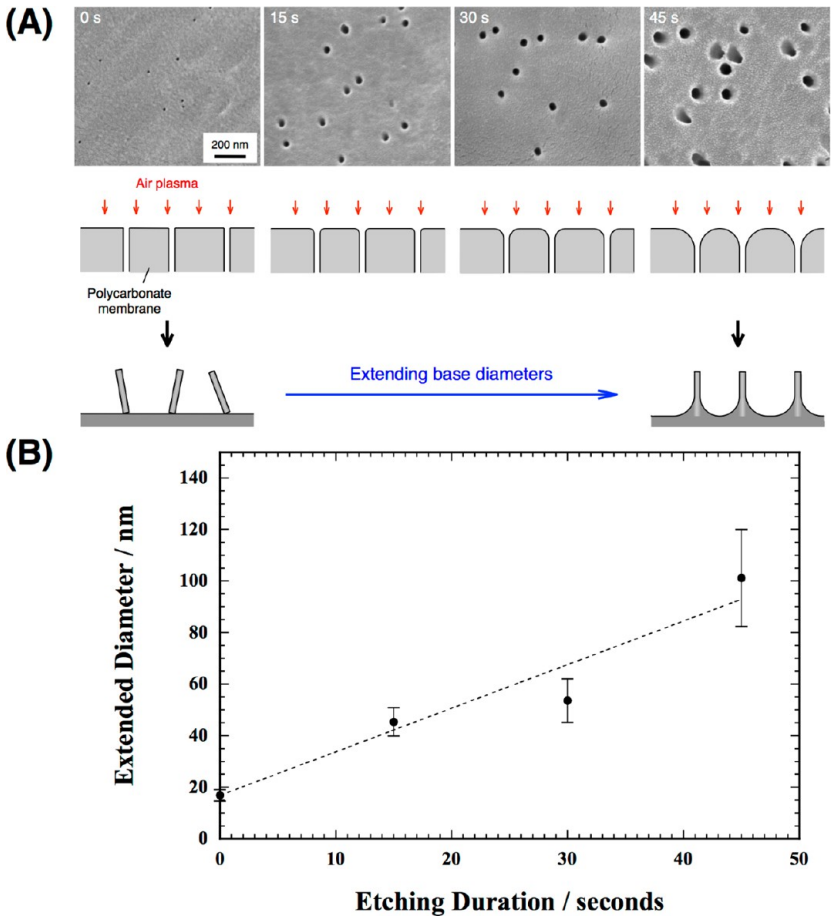

Figure 6. (A) SEM images of polycarbonate membrane surfaces with 15-nm-diameter mouths etched by air plasma for 0, 15, 30, and 45 s with a constant RF power. The illustrations below show how conical pore openings are made by air-plasma etching. As-deposited 15-nm-diameter wires cannot stand without support. Plasma etching of membrane pores leads to extension of the base diameters of NWs. (B) Mouth diameter extended by air-plasma etching as a function of etching duration.

Figure 9 shows a force–distance curve experimentally obtained in the contact-mode AFM with the NW probe in Figure 7B-d. The sample was a polished Si wafer. The relative humidity was controlled to be 7% by dried air.

When a NW probe contacts Si, the vertical deflection of the probe is considered as two springs in series.[23] The following relation is therefore obtained:

$$k_c \Delta z_c = k_n \Delta z_n \quad (2)$$

where k_c is a spring constant of a cantilever beam (=1.7 N m^{-1}) and k_n is a spring constant of a NW in the z direction. Δz_c and Δz_n are respective vertical deflections of a cantilever beam and a NW. After contact, a relative probe displacement, Δz_p, is equal to a sum of two deflections as follows:

$$\Delta z_p = \Delta z_c + \Delta z_n = \left(1 + \frac{k_c}{k_n}\right)\Delta z_c \quad (3)$$

If the axial direction of a wire is perfectly vertical to Si, the wire does not deform until buckling occurs. On the other hand, the lateral spring constant of a NW with a point load at the free end is given by the following equation:[15]

$$k_{tip} = \frac{\pi E}{64}\left[\iint x\left\{d_A + (d_B - d_A)\left(\frac{x}{L}\right)^n\right\}^{-4} dx\, dx\right]^{-1} \quad (4)$$

where E is the Young's modulus (2.1 × 10^{11} Pa for bulk Ni). A k_{tip} of 0.17 N m^{-1} is thus calculated. If a wire pushes Si at a nonvertical angle of θ, the relationship between k_n and k_{tip} is given by

$$k_n \cos^2\theta = k_{tip} \quad (5)$$

From SEM observations, θ was determined to be 67°. Hence,

$$\Delta z_p = 2.5 \Delta z_c \quad (6)$$

The black dashed line with a slope of 1.0 in Figure 9 was measured by a Si AFM probe before electrodeposition of NWs, where only a deflection of the cantilever beam can be assumed. The red dashed line with a slope of 0.40 is drawn by eq 6. The experimental result agrees well with the two-spring model. The maximum load in Figure 9 is approximately 25 nN at the turnaround

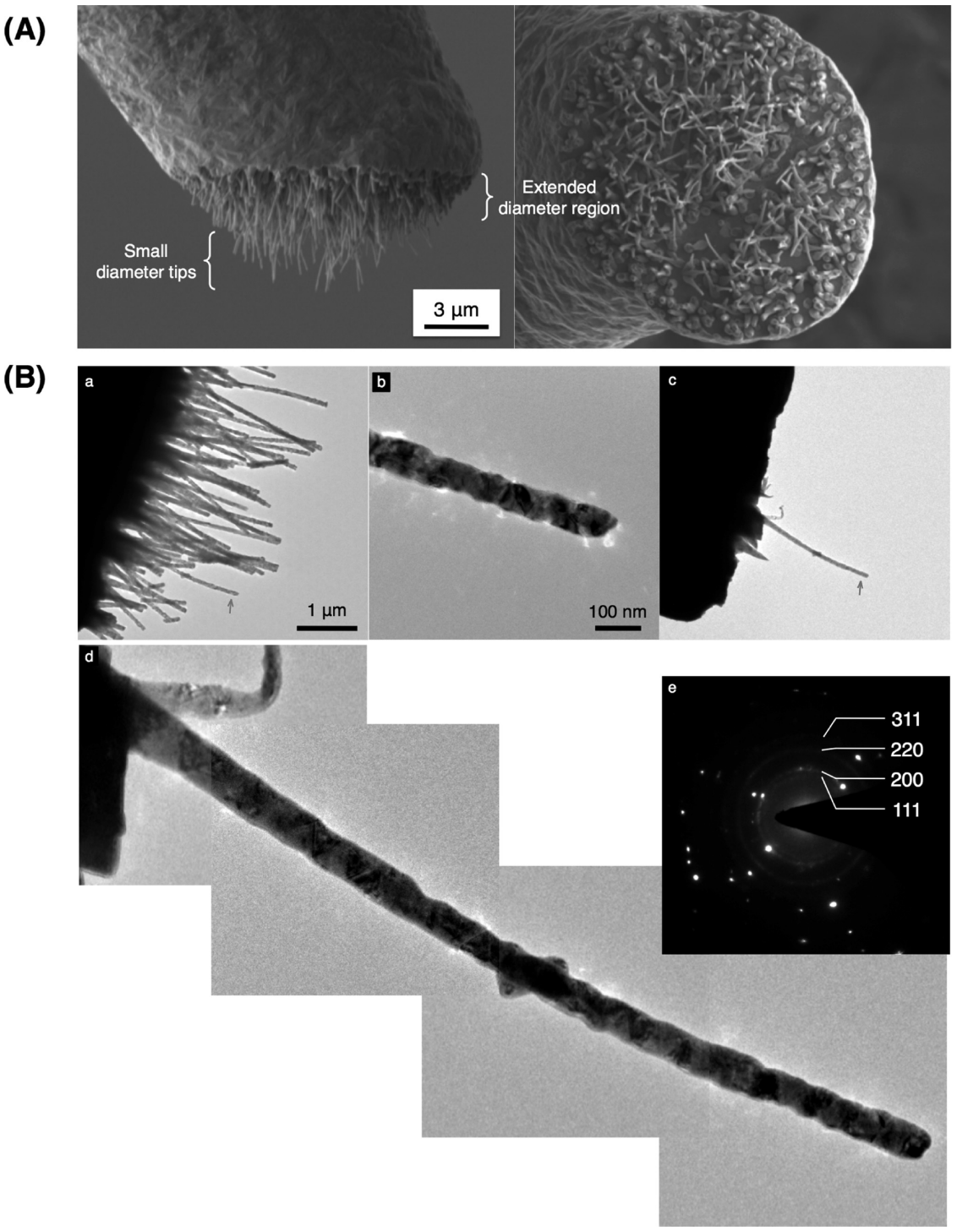

Figure 7. (A) SEM images of Ni NWs on the probe tip electrodeposited using a plasma-etched membrane (original mouth diameter: 15 nm). (B) (a, b) before and (c, d) after FIB etching. The wire indicated by the arrow in (a) was intended to leave. The scale bars in (a) and (b) are common for (b) and (d), respectively. (e) Electron diffraction pattern from the NW tip.

point (the leftmost point in the graph). The adhesion force is approximately 86 nN.

The van der Waals force between a sphere (radius: R) and a flat plane is expressed as follows:[24]

$$F_{vdW} = -\frac{AR}{6D^2} \quad (7)$$

where A is the Hamaker constant and D is the separation distance between two surfaces. The red line in the inset is fit to the experimental plots by eq 7. The best fitting Hamaker constant is 1.1×10^{-19} J (R = 30 nm). This is close to the typical range of Hamaker constants between Si and metals of $(2-5) \times 10^{-19}$ J.[24]

Figure 10A shows calculated stress distributions of the NW in Figure 7B-d using eq 1. A stress becomes

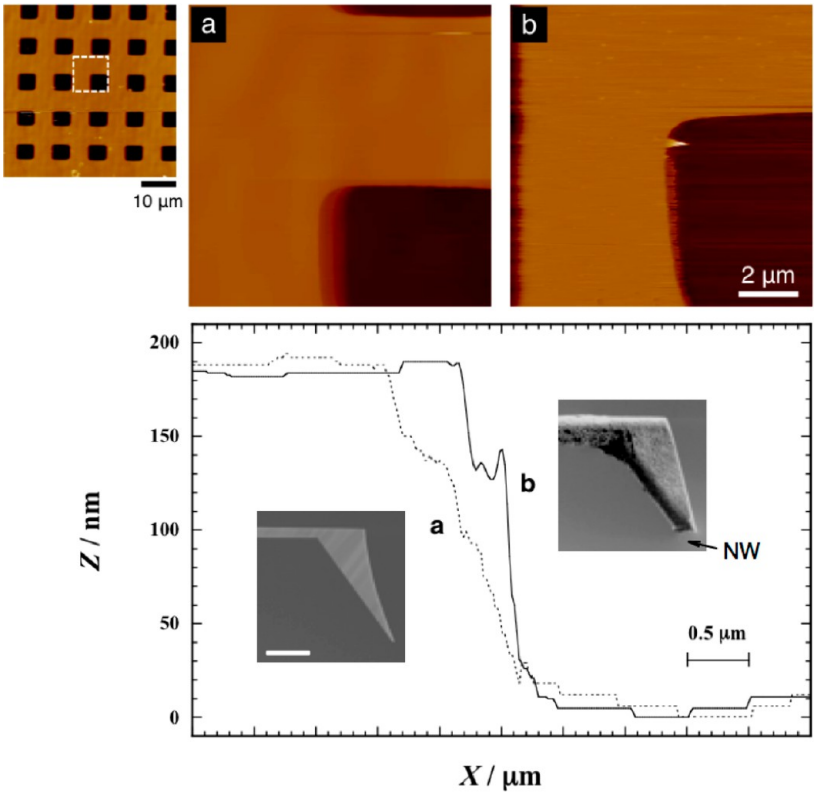

Figure 8. Contact-mode AFM images of a Si grating structure. The top-left image is a topography image of 50 μm $\times$ 50 μm obtained with a Si probe. (a) and (b) are 10 μm $\times$ 10 μm topography images obtained with a Si probe and a single-NW probe, respectively. The bottom figure is height profiles of step edges. The scale bar in an inset is 10 μm.

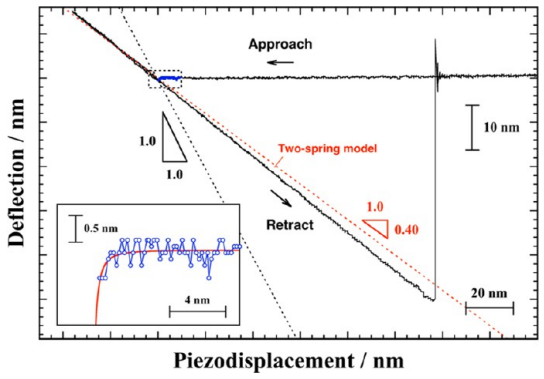

Figure 9. Force−distance curve measured by a single-NW AFM probe in Figure 7B-d. A dotted line with a slope of 1.0 is obtained with a Si probe before growth of NWs. The red dotted line with a slope of 0.40 is almost parallel to the deflection slope for a NW probe. The inset figure shows the deflection variation in the dotted-line square.

maximum at the fixed end when the base diameters are smaller than the free end diameter. However, the position of a maximum stress moves toward the free end as the base diameter increases. When a point load of 1 nN is assumed at the free end, the stress exerted onto the base becomes approximately 7 GPa with a d_B of 15 nm. However, the maximum stress is reduced to 0.04 GPa by extending the d_B to 230 nm. Hence, the NW in Figure 7B-d becomes more than 100 times stiffer than those with a d_B of 15 nm while retaining the small tip radius.

The broken NW probe (Figure 10B-a to d) exhibited that the breaking point corresponded to the position with the maximum stress in Figure 10A. The NW broke at the dashed line between grains A and B in Figure 10B-c. The k_{tip} value of 0.17 N m^{-1} is more than 2 orders of magnitude smaller than the lateral stiffness of the Si_3N_4 tip apexes[25] but a few orders of magnitude greater than those of CNT tips.[26] The shear stress of Ni is reported as one-tenth to one-thirtieth of the shear modulus of 80 GPa.[27,28] If these values are applicable, a vertical load up to approximately 5 $\times$ 10^2 nN can be exerted to this probe based on eq 1.

A summary of comparisons among various kinds of metalized AFM tips is shown in Table 1. The diameters of metal NW tips fabricated in this work are comparable to or even smaller than those of metal-coated CNT tips. Moreover, CNT tips cannot be long with high aspect ratios for the contact-mode applications because of their mechanical instability.[26] On the other hand, a 2-μm-long metal NW tip has demonstrated its ability for contact-mode imaging in this work.

The electrical resistances of single-wall CNTs attached to the AFM tip in the literature are theoretically on the order of kΩ.[34] Metal-coated CNTs should have small electrical resistances on the order of 10 Ω. However, electrons must travel from the CNT tip to the probe chip across a 10^2-μm-long cantilever through a thin metal layer, causing a kΩ-order resistance.[26]

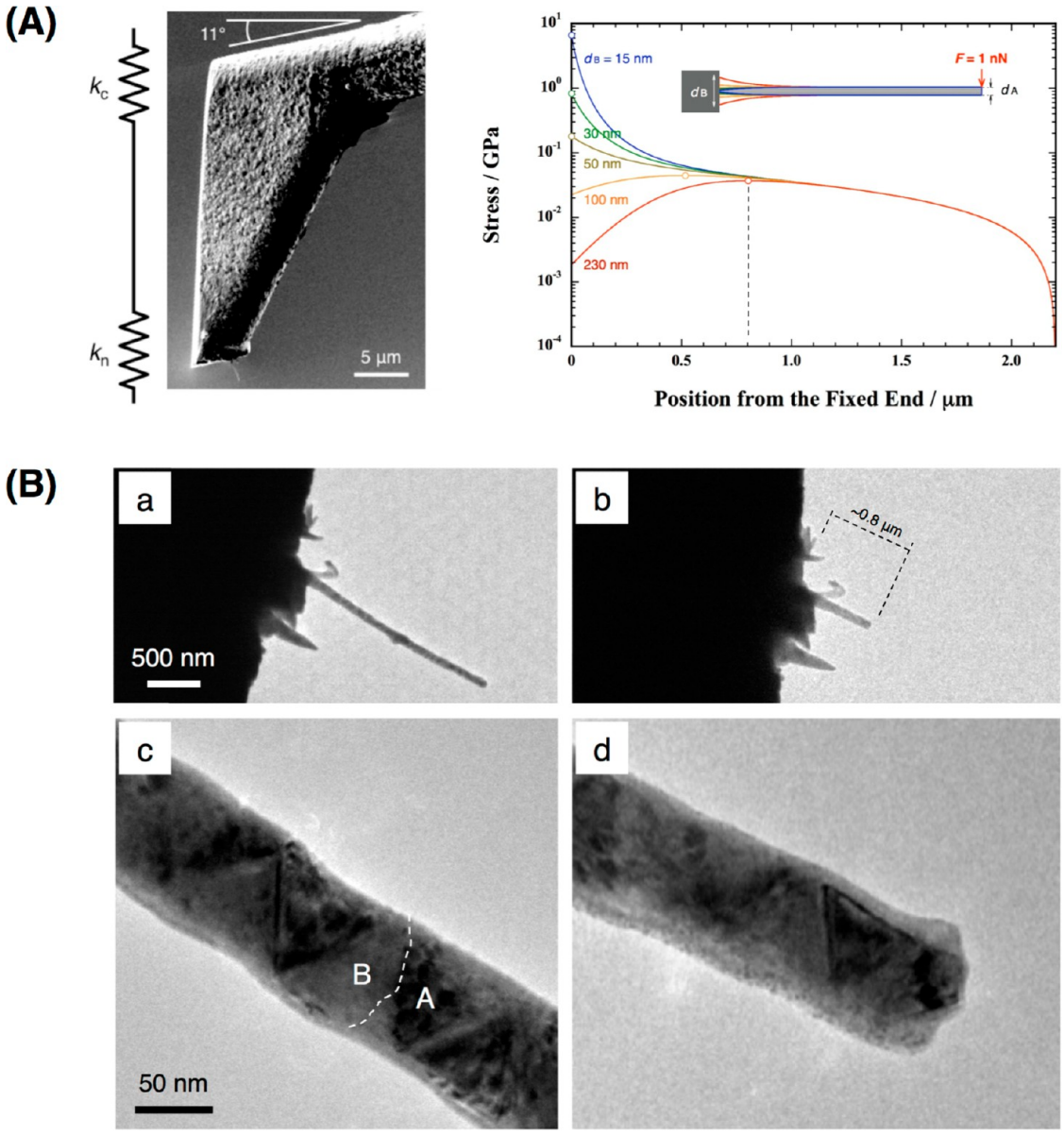

Figure 10. (A) Left: Two springs in series are modeled for a cantilever beam with a NW at the tip. k_c and k_n are explained in the main text. The tilt angle of the probe in the used AFM apparatus is 11 degrees. Right: Stress distributions along the length of a wire with a point load of 1 nN at the free end while the base diameter is increased from 15 to 230 nm. The blank circles indicate the maximum stress positions for the respective base diameters. A wire-shaped profile is assumed by $d_B + (d_A - d_B)(x/L)$.[9] The inset illustrates wire shapes with different base diameters. Each color of a shape profile corresponds to the same color of a stress variation. (B) TEM pictures of the NW tip (a, c) before and (b, d) after breaking. The dashed line between A and B in (c) indicates the broken edge profile in (d).

TABLE 1. Comparison of Metalized AFM Tips

	imaging mode	tip diameter	metal layer thickness	length of vertical portion	ref
metal-coated Si tips	contact/tapping	>30 nm	10–70 nm	conical	29–31
metal-coated CNT tips	contact/tapping	50–100 nm	20–25 nm	contact: <250 nm tapping: >1 μm	26, 32
metal-infiltrated CNT tips	tapping	~100 nm		>10 μm	33
metal NW tips	contact	15–70 nm	whole	>2 μm	this work

With a thick metal coating, the tip radius increases. Regardless of total electrical resistance, the metal layer at the tip of a CNT seems to be hardly wear resistant. Metal NW AFM probes resolve this critical problem of metal-coated CNT tips. Moreover, the electrode potential measurements in electrolytes were successfully demonstrated by the NW tip in this work. Hence, AFM probes with template-grown-metal NWs are superior

to metal-coated CNT tips in several important aspects, such as mechanical robustness, risk of wearing, and aspect ratio, at least for the contact-mode applications.

CONCLUSIONS

Fabrication of single-metal-NW probes has been demonstrated in this report. Arrays of NWs were electrodeposited by the porous-template method on the tip of an AFM probe. Subsequently, NWs were removed by FIB, enabling the realization of single NWs. Redeposition accompanying FIB etching was prevented by tightly controlling the ion beam direction. Plasma etching successfully extended pore sizes only at openings of polymer membranes. Free-standing NWs were electrodeposited even with membranes of 15-nm-diameter pores. Consequently, metal NW tips can be superior scanning probes to metal-coated CNT tips for contact-mode applications. The mechanical behavior of AFM tips was established, and their functionality including electrical and electrochemical behavior was demonstrated.

METHODS

Electrochemical deposition of NWs was conducted using polycarbonate-track-etched membranes (Toyo Roshi Kaisha, Ltd.; Nomura Micro Sci. Co.) The pore diameters were 15 nm (number density: 6×10^8 cm^{-2}) to 100 nm (4×10^8 cm^{-2}). The membrane thicknesses were 6.0 μm. When 15-nm-diameter pores were used, one surface of a membrane was air-plasma-etched. The electrolyte composition was 1.0 M $NiSO_4$, 0.19 M $NiCl_2$, and 0.62 M H_3BO_3 (pH 3.4). The applied potential was -0.9 V with respect to a Ni wire reference electrode. Commercial contact-mode Si-AFM probes (NANOSENSORS AdvancedTEC) were used as substrates of NWs. The tip of purchased AFM probes was originally angled ahead of the beam front.[15] The 3-nm-thick Cr and 20-nm-thick Au films were sequentially sputter-deposited onto the tip side of an AFM probe. The other side of a cantilever beam was coated with a thin epoxy layer to prevent Ni growth because a laser light needed to be reflected there in AFM measurements. The counter electrode was a Ni sheet. The deposition duration was 150 s.

After electrodeposition, dichloromethane (CH_2Cl_2) was slowly added into the electrolyte. A separate phase of dichloromethane formed under an aqueous electrolyte layer due to density differences. Consequently, an AFM probe was submerged in the dichloromethane phase. The template membrane was removed at this step. The sample was quickly taken out and kept in a vessel with fresh dichloromethane for a couple of hours. Finally, remaining epoxy layers on the sample were removed by air plasma followed by rinsing with acetone and 2-propanol. The last two procedures were repeated as necessary. A dual-beam FIB/SEM instrument (FEI) was used to produce single NWs on the probe tip. Contact-mode AFM measurements were performed with a scan duration of 1.0 s for every single line in a captured frame (total 512 lines) in dried air (7% relative humidity) at room temperature.

Conflict of Interest: The authors declare no competing financial interest.

Acknowledgment. The authors gratefully acknowledge Dr. Ann F. Marshall for technical support on the TEM.

REFERENCES AND NOTES

1. Whitney, T. M.; Jiang, J. S.; Searson, P. C.; Chien, C. L. Fabrication and Magnetic Properties of Arrays of Metallic Nanowires. *Science* **1993**, *261*, 1316–1319.
2. Martin, C. R. Nanomaterials - a Membrane-Based Synthetic Approach. *Science* **1994**, *266*, 1961–1966.
3. Brumlik, C. J.; Martin, C. R. Template Synthesis of Metal Microtubules. *J. Am. Chem. Soc.* **1991**, *113*, 3174–3175.
4. Zach, M. P.; Ng, K. H.; Penner, R. M. Molybdenum Nanowires by Electrodeposition. *Science* **2000**, *290*, 2120–2123.
5. Nishizawa, M.; Menon, V. P.; Martin, C. R. Metal Nanotubule Membranes with Electrochemically Switchable Ion-Transport Selectivity. *Science* **1995**, *268*, 700–702.
6. Salem, A. K.; Searson, P. C.; Leong, K. W. Multifunctional Nanorods for Gene Delivery. *Nat. Mater.* **2003**, *2*, 668–671.
7. Liu, Z.; Searson, P. C. Single Nanoporous Gold Nanowire Sensors. *J. Phys. Chem. B* **2006**, *110*, 4318–4322.
8. Piraux, L.; Renard, K.; Guillemet, R.; Mátéfi-Tempfli, S.; Mátéfi-Tempfli, M.; Antohe, V. A.; Bouzehouane, S. K.; Cros, V. Template Grown NiFe/Cu/NiFe Nanowires for Spin Transfer Devices. *Nano Lett.* **2007**, *7*, 2563–2567.
9. Motoyama, M.; Fukunaka, Y.; Sakka, T.; Ogata, Y. H.; Kikuchi, S. Electrochemical Processing of Cu and Ni Nanowire Arrays. *J. Electroanal. Chem.* **2005**, *584*, 84–91.
10. Yazdanpanah, M. M.; Harfenist, S. A.; Safir, A.; Cohn, R. W. Selective Self-Assembly at Room Temperature of Individual Freestanding Ag_2Ga Alloy Nanoneedles. *J. Appl. Phys.* **2005**, *98*, 73510.
11. Hu, J.; Yu, M.-F. Meniscus-Confined Three-Dimensional Electrodeposition for Direct Writing of Wire Bonds. *Science* **2010**, *329*, 313–316.
12. Feng, G.; Nix, W. D.; Yoon, Y.; Lee, C. J. A Study of the Mechanical Properties of Nanowires Using Nanoindentation. *J. Appl. Phys.* **2006**, *99*, 074304.
13. Wu, B.; Heidelberg, A.; Boland, J. J. Mechanical Properties of Ultra-High Strength Gold Nanowires. *Nat. Mater.* **2005**, *4*, 525–529.
14. Chen, C. Q.; Shi, Y.; Zhang, Y. S.; Zhu, J.; Yan, Y. J. Size Dependence of Young's Modulus in ZnO Nanowires. *Phys. Rev. Lett.* **2006**, *96*, 075505.
15. Motoyama, M.; Dasgupta, N. P.; Prinz, F. B. Electrochemical Deposition of Metallic Nanowires as a Scanning Probe Tip. *J. Electrochem. Soc.* **2009**, *156*, D431–D438.
16. Giannuzzi, L. A.; Stevie, F. A. *Introduction to Focused Ion Beams - Instrumentation, Theory, Technique and Practice*; Springer Science: New York, 2005.
17. Belson, J.; Wilson, I. H. Theory of Redeposition of Sputtered Flux on to Surface Asperities. *Nucl. Instrum. Methods* **1981**, *182*, 275–281.
18. Schönenberger, C.; van der Zande, B. M. I.; Fokkink, L. G. J.; Henny, M.; Schmid, C.; Krüger, M.; Bachtold, A.; Huber, R.; Birk, H.; Staufer, U. Template Synthesis of Nanowires in Porous Polycarbonate Membranes: Electrochemistry and Morphology. *J. Phys. Chem. B* **1997**, *101*, 5497–5505.
19. Apel, P. Y.; Blonskaya, I. V.; Dmitriev, S. N.; Mamonova, T. I.; Orelovitch, O. L.; Sartowska, B.; Yamauchi, Y. Surfactant-Controlled Etching of Ion Track Nanopores and Its Practical Applications in Membrane Technology. *Radiat. Meas.* **2008**, *43*, S552–S559.
20. Yu, S.; Li, N.; Wharton, J.; Martin, C. R. Nano Wheat Fields Prepared by Plasma-Etching Gold Nanowire-Containing Membranes. *Nano Lett.* **2003**, *3*, 815–818.
21. Gere, J. M. *Mechanics of Materials*, 6th ed.; Brooks/Cole-Thomas Learning: Belmont, 2004.
22. Sader, J. E.; Chon, J. W. M.; Mulvaney, P. Calibration of Rectangular Atomic Force Microscope Cantilevers. *Rev. Sci. Insrum.* **1999**, *70*, 3967–3969.
23. Villarrubia, J. S. In *Applied Scanning Probe Methods*; Bhushan, B.; Funds, H.; Hosaka, S., Eds.; Springer-Verlag: Berlin, 2004.
24. Israelachvili, J. N. *Intermolecular and Surfaces Forces*, 3rd ed.; Elsevier, 2011; p 354.
25. Lantz, M. A.; O'Shea, S. J.; Hoole, A. C. F.; Welland, M. E. Lateral Stiffness of the Tip and Tip-Sample Contact in

Frictional Force Microscopy. *Appl. Phys. Lett.* **1997**, *80*, 970–972.
26. Wilson, N. R.; Macpherson, J. V. Single-Walled Carbon Nanotubes as Templates for Nanowire Conducting Probes. *Nano Lett.* **2003**, *3*, 1365–1369.
27. Lund, A. C.; Schuh, C. A. Strength Asymmetry in Nanocrystalline Metals under Multiaxial Loading. *Acta Mater.* **2005**, *53*, 3193–3205.
28. Srinivasan, S. G.; Baskes, M. I. Atomistic Simulations of the Plasticity Behavior of Shock-Induced Polycrystalline Nickel. *Metall. Mater. Trans. A* **2007**, *38*, 2716–2720.
29. http://www.nanoworld.com (Nanoworld Corporation).
30. Hudson, J. E.; Abruña, H. D. Electrochemically Controlled Adhesion in Atomic Force Spectroscopy. *J. Am. Chem. Soc.* **1996**, *118*, 6303–6304.
31. Beebe, J. M.; Engelkes, V. B.; Miller, L. L.; Frisbie, C. D. Contact Resistance in Metal-Molecule-Metal Junctions Based on Aliphatic SAMs: Effects of Surface Linker and Metal Work Function. *J. Am. Chem. Soc.* **2002**, *124*, 11268–11269.
32. Burt, D. P.; Wilson, N. R.; Weaver, J. M. R.; Dobson, P. S.; Macpherson, J. V. Nanowire Probes for High Resolution Combined Scanning Electrochemical Microscopy-Atomic Force Microscopy. *Nano Lett.* **2005**, *5*, 639–643.
33. Wolny, F.; Weissker, U.; Mühl, T.; Leonhardt, A.; Menzel, S.; Winkler, A.; Büchner, B. Iron-Filled Carbon Nanotubes as Probes for Magnetic Force Microscopy. *J. Appl. Phys.* **2008**, *104*, 0649081–0649085.
34. Wilson, N. R.; Cobden, D. H.; Macpherson, J. V. Single-Wall Carbon Nanotube Conducting Probe Tips. *J. Phys. Chem. B* **2002**, *106*, 13102–13105.